Quantum cascade laser thermal therapy guided by FDOCT

Yong Huang (黄 勇)* and Jin U. Kang

Department of Electrical and Computer Engineering, Johns Hopkins University, 3400 N. Charles Street, Baltimore, MD, 21210, USA

**Corresponding author: yhuang60@jhu.edu*

Received October 30, 2012; accepted November 19, 2012; posted online December 26, 2012

We demonstrate Fourier domain optical coherenc tomography (FDOCT) monitoring and guiding of quantum cascade laser (QCL) therapy. The laser therapy is performed with a 6.1-μm mid-IR QCL and it involves both tissue coagulation or ablation. FDOCT allows real-time monitoring that minimize unnecessary damage to the surrounding tissues. We perform lipid phantom tissue ablation, chicken egg yolk coagulation, and tissue and blood vessel coagulation on chicken embryo to validate the FDOCT guiding quantum cascade laser therapy.

OCIS codes: 110.4500, 170.3880, 170.6930.
doi: 10.3788/COL201311.011701.

Medical lasers have become an integral part of the modern medicine[1]. Laser based procedures such as UV ArF excimer laser ablation of corneal stroma during laser refractive surgery, green argon laser photo coagulation for retinal detachment and diabetic retinopathy[2], and Nd:YAG laser tumor resection[3] are being widely used. However precise laser therapy with a minimal thermal damage to the surrounding regions requires careful power control and monitoring. Also optimized wavelength setting can greatly minimize collateral damage. Most soft-tissues have high water (up to 65%) and protein (up to 35%) content. Therefore water and protein absorption coefficient are two important factors that determine which wavelength to use. High water absorption coefficient in the IR range makes IR lasers a good candidate for high-precision bio-tissue ablation. In the mid-IR range, wavelengths of 6.1 and 6.45 μm fall within the absorption peaks of amide protein groups, Amide-I and Amide-II, respectively[4]. The absorption peak at 6.1 μm also coincides with the deformation mode of water. However there has not been a practical source in that wavelength band until recently with an advent of quantum cascade lasers (QCLs) which are compact and highly efficient[5]. Over the past several years, there have been significant improvement in their power and stability[6]. QCLs are also low cost, compact size, and tunable which makes them a great alternative tunable free-electron-laser (FEL) and optical parametric oscillators (OPOs). In the IR range when a train of pulses of laser light is focused on a biological tissue, laser radiation is absorbed by the target tissue, which results in the significant local temperature increase. Thermal coagulation of irradiated soft-tissue and denaturation of proteins will occur when the temperature increases above 60 °C. Ablation will occur when temperature goes up high enough to induce explosive evaporation of cellular water.

To precisely guide laser therapy various image-based monitoring systems include magnetic resonance imaging[7], computer tomography[8], and ultrasound[9] are being used. However, limitations such as low image resolution, slow imaging speed, and complexity prevent effective real-time therapy guidance[10]. Optical coherence tomography (OCT) is an established, non-invasive optical imaging technology that can provide high-speed, high-resolution, and 3D images of biological samples. Since early 1990s, OCT has been widely used for diagnosis, therapy monitoring, and ranging[11,12]. OCT guided laser therapy can deliver a real-time monitoring system that avoids unnecessary damage to surrounding tissues. We recently performed tissue ablation and coagulation using a 6.12-μm QCL[13]. In this study, we demonstrated several QCL based laser therapy procedures with real-time feedback from OCT system to optimize laser treatment.

We used a pulsed QCL system (AdTech, USA) operating at temperature of 293 K to perform the studies (Fig. 1). The laser operated at a peak output power of 791.7 mW at 2.1 A/15.3 V. A lens system (F=25.4 mm, LB5774, Thorlabs) was used to focus the light onto the sample. The sample was placed on a 3D translation stage. We used a in-house built spectral-domain OCT (SD-OCT) system to performed the OCT monitoring and guiding. The OCT has a lateral resolution of 15 μm and an effective axial resolution of 3.6 μm in air and 2.8 μm in water. The system operates at 70 000 A-scans per second and can be switched between B-mode and C-mode imaging. Each B-frame consists of 1 000 A-scans and 256 B-frames forms a C-mode volume. Each B-mode and volume acquisition time were 0.014 and 3.7 s,

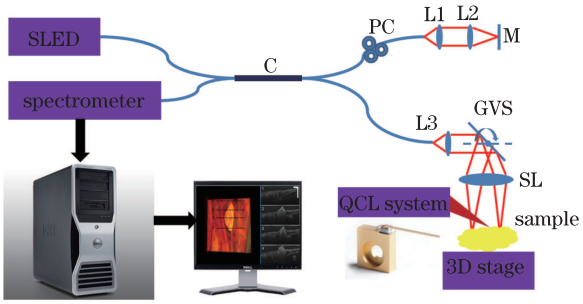

Fig. 1. System configuration (C: 50/50 coupler; PC: polarization controller; M: reference mirror; L1, L2, L3: achromatic focal lenses; SL: scanning lens; GVS: galvanometer scanning mirror pair).

respectively. The real-time data processing and visualization was accelerated by our customized software using graphics processing unit (GPU)[14]. This fast 3D image feedback of the targeted area enables responsive evaluation of the laser therapy outcome and laser dosimetry.

We performed a series of laser therapy using several phantoms to evaluate the OCT guided 6.1-μm QCL procedures. We performed a lipid phantom ablation study under different pulse length and pulse number conditions. The laser driving current was set at 750 mA, which corresponded to 163-mW peak optical power. The pulse length was set at three different values: 20, 50, and 100 ms. The laser beam was focused to a 0.2-mm beam diameter on the phantom surface. The laser power density was 532 W/cm^2. The number of pulses applied to the target was either 1, 2, 3 or 10 pulses. Figure 2(a) shows *en-face* projection of OCT acquired volume image data set, after the lipid phantom has been exposed to different amount of laser pulses. From the *en-face* image we can clearly see the ablated sites with different radii induced by laser

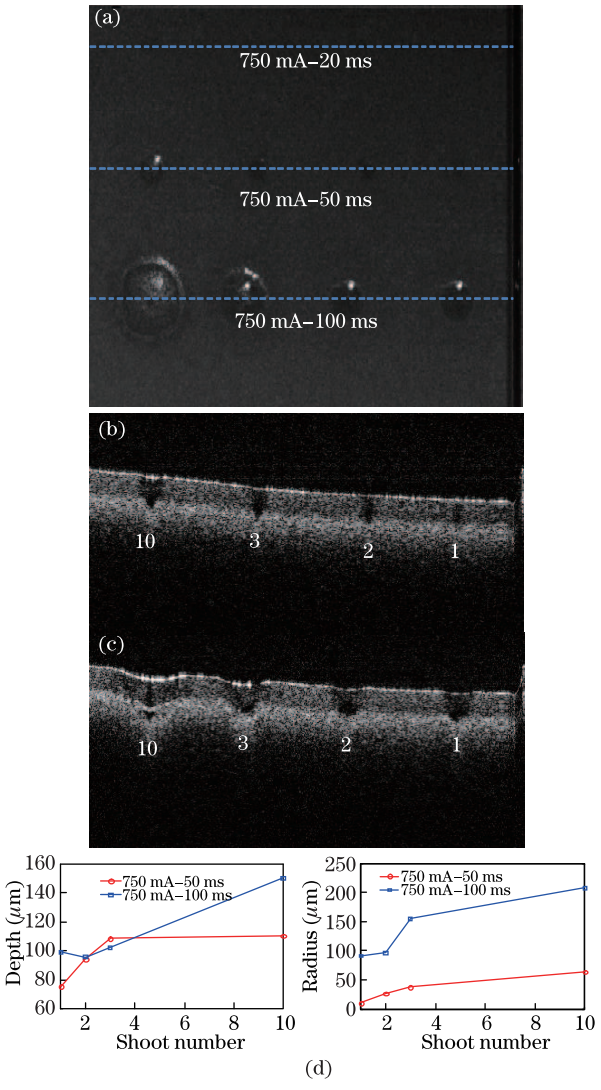

Fig. 2. Lipid Phantom Ablation. (a) *En-face* project image of ablated area (H×W: 2×2.67 (mm)); (b) crossectional image of line 750 mA–50 ms; (c) crossectional image of line 750 mA–100 ms; (d) depth and radius of ablated sites under different laser conditions.

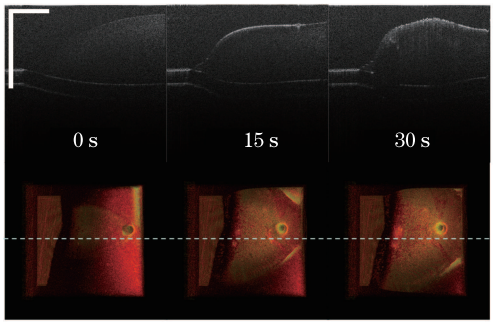

Fig. 3. Chicken egg yolk coagulation via laser radiation over 30 s, top row are the corresponding B-mode images of the dashed line on the bottom top-view volume rendering images of the scanned area (scale bar: 500 μm; color image size H×W: 1×2 (mm)).

pulses. Figures 2(b) and (c) show the crossectional image corresponding to the dashed lines on Fig. 2(a). The number of pulses applied to the tissue site indicated by the numbers on the image. From Figs. 2(a)–(c), the depth and radius of the ablated site can be quantitatively assessed and this is summarized in Fig. 2(d). It clearly shows increasing depth and radius of the ablation with the increasing pulse length and pulse number. There is, however, a saturation effect with the number of pulses.

We then performed soft-tissue and blood vessel coagulations using chicken embryo model. For this study the laser operated at current level of 1.3 A, which corresponded to a 440 mW peak optical power with pulse length of 30 ms and repetition rate of 20 Hz.

Screen captured images of the chicken egg yolk coagulation at different time points over a 30 s period is shown in Fig. 3. The laser beam diameter was 1 mm on the sample surface. The B-mode cross-sectional images corresponds to the midpoint of the 3D volume images. From the B-mode images we can assess the gradual formation of the tissue coagulation. The coagulated tissue is indicated by increased density and thus increased signal intensity.

We further evaluated soft-tissue and blood vessel coagulation using the chicken embryo model. The chorioallantoic membrane (CAM) of chick embryo is a well-established model for studying microvasculature and has been used extensively to investigate the effects of vasoactive drugs, optical and thermal processes in blood vessels, as well as retina simulation[15]. Figure 4 shows a coagulated soft-tissue lesion created by laser radiation having beam diameter of 0.5 mm on the surface surrounded by healthy tissue. Left color image is the top-view volume rendering image, and right four images are B-mode crossectional images corresponding to the line position marked on the left color image. From the OCT top-view volume rendering image, we can clearly identify the morphology and size of the lesions. Combined with the B-mode crossectional images, we can assess the depth of the tissue coagulation. The real-time imaging feedback can help the surgeon determine precisely when to terminate the laser radiation.

Figure 5 shows the blood vessel coagulation test with QCL. Figures 5(a) and (b) are the crossectional image at position marked by black lines in Figs. 5(c) and (d) respectively. Figures 5(c) and (d) are the top-view volume

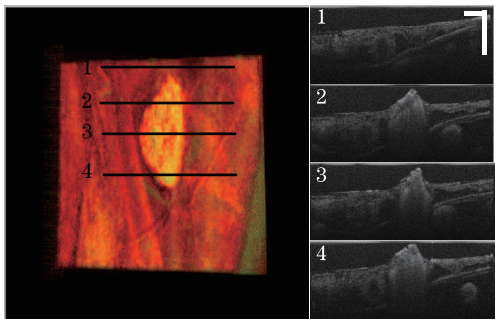

Fig. 4. Soft-tissue coagulation in chicken embryo (scale bar: 250 μm; color image size H×W: 1×2 (mm)).

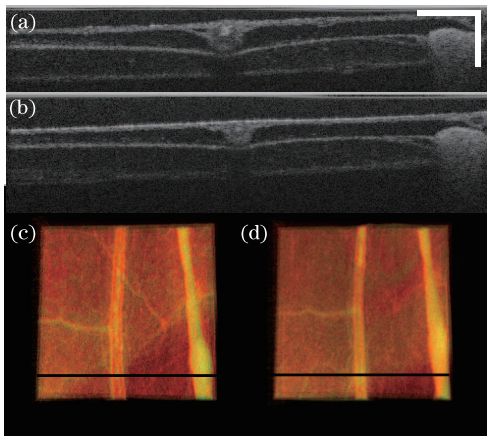

Fig. 5. Blood vessel coagulation. (a) Crossectional image corresponding to dashed line in (c); (b) crossectional image corresponding to dashed line in (d); (c) top-view volume rendering image of area of interest before laser radiation; (d) top-view volume rendering image of area of interest after laser radiation for 1 min (scale bar: 250 μm; color image size H×W: 1×2 (mm)).

rendering image of the acquired 3D data. Figure 5(c) is before laser radiation while Fig. 5(d) is after laser radiation with a beam diameter of 2 mm for 1 min. Comparing Figs. 5(c) and (d) we can see the central blood vessel gets thinned and membrane surface gets clean as some tiny soft-tissue structure was also coagulated. This can also be confirmed by comparing Figs. 5(a) and (b). We can see the crossectional vessel size has decreased and the top membrane surface gets thinner and more uniform from Figs. 5(a) to (b).

In conclusion, we demonstrate for the first time to the best of our knowledge real-time FDOCT monitoring and assessment of a 6.1-μm QCL laser procedures such as lipid phantom tissue ablation, tissue and blood vessel coagulation using chicken embryo model. The results shows that the FDCOT can be highly effective in determining the size and the effectiveness of mid-IR laser based tissue coagulation and ablation.

This work was supported by NSF ERC (MIRTHE). Yong Huang is partially supported by China Scholarship Council (CSC). We would like to thank AdTech Optics and Dr. Janyu Fan for providing us the laser and fruitful discussion.

References

1. M. H. Niemz, *Laser-Tissue Interactions*: *Fundamentals and Applications* (Springer-Verlag, Berlin, 2007).
2. S. S. Hayreh, M. R. Klugman, P. Podhajsky, G. E. Servais, and E. S. Perkins, Graefes Arch. Clin. Exp. Ophthalmol. **228,** 281 (1990).
3. S. V. Esser, G. Stapper, P. J. V. Diest, M. A. A. J. V. D. Bosch, J. H. G. M. Klaesens, W. P. Th. M. Mali, I. H. M. B. Rinkes, and R. V. Hillegersberg, Ann. Surg. Oncol. **16,** 2259 (2009).
4. V. A. Serebryakov, E. V. Boiko, N. N. Petrishchev, and A. V. Yan, J. Opt. Technol. **77,** 6 (2010).
5. J. Faist, F. Capasso, D. L. Sivco, C. Sirtori, A. L. Hutchinson, and A. Y. Cho, Science **264,** 553 (1994).
6. Y. Yao, A. J. Hoffman, and C. F. Gmachl, Nat. Photon. **6,** 432 (2012).
7. Y. C. Chen, S. C. Gnyawali, F. Wu, H. Liu, Y. A. Tesiram, A. Abbott, R. A. Towner, and W. R. Chen, J. Biomed. Opt. **13,** 044033 (2008).
8. G. V. Maltzahn, J. H. Park, A. Agrawal, N. K. Bandaru, S. K. Das, M. J. Sailor, and S. N. Bhatia, Canc. Res. **69,** 3892 (2009).
9. D. Oepkes, R. Devlieger, E. Lopriore, and F. J. C. M. Klumper, Ultrasound Obstet. Gynecol. **29,** 457 (2007).
10. S. A. Boppart, J. Herrmann, C. Pitris, D. L. Stamper, M. E. Brezinski, and J. G. Fujimoto, J. Surg. Res. **82,** 275 (1999).
11. W. Drexler and J. G. Fujimoto, *Optical Coherence Tomography*: *Technology and Applications* (Springer-Verlag, Berlin, 2008).
12. B. J. Vakoc, G. J. Tearney, and B. E. Bouma, J. Biomed. Opt. **12,** 020501 (2007).
13. Y. Huang and J. U. Kang, Proc. SPIE **8209,** 82091W (2012).
14. Y. Huang, X. Liu, and J. U. Kang, Biomed. Opt. Express **3,** 2162 (2012).
15. T. Leng, J. M. Miller, K. V. Bilbao, D. V. Palanker, P. Huie, and M. S. Blumenkranz, Retina **24,** 427 (2004).